A novel mathematical model for controllable near-field electrospinning

Cite as: AIP Advances **4**, 017108 (2014); https://doi.org/10.1063/1.4861705
Submitted: 17 October 2013 . Accepted: 16 December 2013 . Published Online: 03 January 2014

Changhai Ru, Jie Chen, Zhushuai Shao, Ming Pang, and Jun Luo

A novel mathematical model for controllable near-field electrospinning

Changhai Ru,[1,2,a] Jie Chen,[2] Zhushuai Shao,[2] Ming Pang,[1] and Jun Luo[3,a]
[1]*College of Automation, Harbin Engineering University, Harbin 150001, China*
[2]*Robotics and Microsystems Center, Soochow University, Suzhou 215021, China*
[3]*School of Mechatronics Engineering and Automation, Shanghai University, Shanghai 200072, China*

(Received 17 October 2013; accepted 16 December 2013; published online 3 January 2014)

Near-field electrospinning (NFES) had better controllability than conventional electrospinning. However, due to the lack of guidance of theoretical model, precise deposition of micro/nano fibers could only accomplished by experience. To analyze the behavior of charged jet in NFES using mathematical model, the momentum balance equation was simplified and a new expression between jet cross-sectional radius and axial position was derived. Using this new expression and mass conservation equation, expressions for jet cross-sectional radius and velocity were derived in terms of axial position and initial jet acceleration in the form of exponential functions. Based on Slender-body theory and Giesekus model, a quadratic equation for initial jet acceleration was acquired. With the proposed model, it was able to accurately predict the diameter and velocity of polymer fibers in NFES, and mathematical analysis rather than experimental methods could be applied to study the effects of the process parameters in NFES. Moreover, the movement velocity of the collector stage can be regulated by mathematical model rather than experience. Therefore, the model proposed in this paper had important guiding significance to precise deposition of polymer fibers. [http://dx.doi.org/10.1063/1.4861705]

I. INTRODUCTION

Electrospinning is a convenient, cheap and straightforward method to produce fibers from polymer solutions and melts. These polymer fibers are of intense scientific and industrial interests due to their unique characteristics such as small diameters, large surface area to volume ratio and superior physical and chemical properties. As the process has so many considerable advantages, it has been investigated for a wide range of applications, such as electrospun membranes for filtration,[1] bio-scaffolds,[2] solar energy applications,[3] wound dressing,[4] drug delivery systems,[5] sensors[6] and piezoelectric nanofibrous devices[7] etc. Due to the existence of the electrical potential difference between the pendant droplet of polymer solutions and a grounded collector, the droplet acquires a stable shape if the potential has not reached the critical value. When the potential difference is increased, the surface of the droplet becomes charged with its shape altering from a circular to a conical one referred to as the Taylor cone.[8] When the potential difference is high enough that the electrical force imposed on the liquid droplet overcomes the surface tension force, a stable electrified jet emerges. The electrospinning process typically involves two stages. In the first stage, the polymer jet travels in a straight line for a few seconds, in the second stage, a "bending instability" occurs and the jet begins to curl and spiral in space.[9] Due to the inherent instability of far-field electrospinning (FFES), its controllability is limited. Although many methods have been developed to gain aligned

[a]Corresponding author: rchhai@gmail.com and luojun@shu.edu.cn

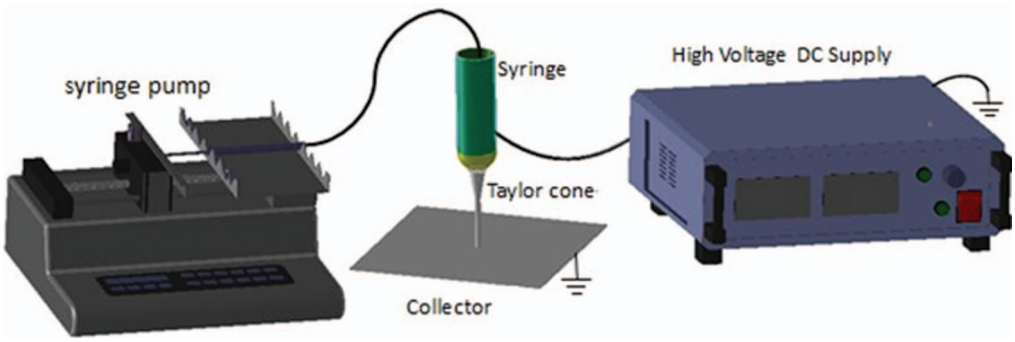

FIG. 1. Schematic of experimental setup for NFES

nanofibers, including manipulating electric field lines[10–14] and utilization of a rotating device,[15] it remains difficult to deposit polymer fibers precisely.

In 2006, Sun and Lin[16] reported a new type of electrospinning called near-field electrospinning (NFES), the schematic of experimental setup for NFES is explained in Figure 1. In NFES, the pipette-collector distance is reduced to the range of 500 μm to 3 mm to utilize the stable stage of electrospinning. However, there are two problems existing in NFES. On one hand, due to the lack of stretching and splitting of the charged jet in the second stage of electrospinning, fibers of nanoscale can not be acquired. On the other hand, to collect precisely deposited polymer fibers, the collector stage should move at an appropriate velocity. But due to the lack of guidance of theoretical model, the movement velocity of the collector stage can only be adjusted by experience. In order to produce polymer fibers, Chieh Chang *et al.*[17] and Bisht *et al.*[18] used a probe tip to draw a single fiber from the droplet mechanically to initiate continuous NFES, which decreased the initial jet cross-sectional radius as well as the applied voltage. But due to the lack of theoretical model, they could only conduct their experiments by experience. In this paper, a mathematical model has been proposed which has important guiding significance to precise deposition of polymer fibers in NFES. Firstly, it will be able to accurately predict the diameter and velocity of polymer fibers in NFES. Secondly, it will be able to apply mathematical analysis rather than experimental methods to study the effects of the process parameters in NFES. Thirdly, the movement velocity of the collector stage will be able to be regulated according to mathematical model rather than experience. Therefore, with the proposed model, it will be more accurate and convenient to deposit precisely polymer fibers in NFES.

In section II, three unknown quantities of the charged jet in NFES, namely the jet cross-sectional radius, jet velocity and jet acceleration are formulated in the form of exponential functions in terms of axial position and initial jet acceleration. In section III, based on Slender-body theory and Giesekus model, a quadratic equation for initial jet acceleration was acquired. The results of the theoretical predictions are compared with experimental data in section IV. In section V, the conclusions are given.

II. DERIVATION OF JET CROSS-SECTIONAL RADIUS AND VELOCITY

In near-field electrospinning, the electrified jet travels in a nearly straight line, therefore, the liquid jet can be assumed to be extensional and axisymmetric in the direction of the external electric field. After getting stable, the movement of the electrified jet in the electric field can be seen as one dimensional steady-state. One dimensional steady-state fluid model is used to analyze the behavior of the jet. Three equations representing mass conservation, charge conservation and the linear momentum balance are provided.[19]

$$\pi r^2 v = Q \tag{1}$$

$$2\pi r\sigma v + k\pi r^2 E = I \tag{2}$$

$$\frac{d}{dz}\left(\frac{v^2}{2}\right) = -\frac{1}{\rho}\frac{dp}{dz} + g + \frac{2\sigma E}{\rho r} + \frac{d\tau}{dz} \tag{3}$$

Where Q is a constant volume flow rate, ρ is the density of the jet, v is the jet velocity, r is the cross-sectional radius, E is the z component of the electric field, I is the total current in the electrified jet, τ is the axial viscous stress, k is the electric conductivity of the liquid jet and σ is the surface charge density. In near-field electrospinning, the electrical forces imposed on the jet far overweigh the other forces, such as the gravity, inertial, viscous, surface tension and hydrostatic forces. Therefore, Eq. (3) can be reduced to the following expression.

$$\frac{d}{dz}\left(\frac{v^2}{2}\right) = \frac{2\sigma E}{\rho r} \tag{4}$$

Because the electric current in the jet I and the volumetric flow rate Q are considered external parameters of the model and are assumed to be constant, Eqs. (5) and (6) can be derived from Eqs. (1), (2) and (4).

$$v \propto r^{-2}, \sigma \propto r, E \propto r^{-2} \tag{5}$$

$$\frac{d}{dz}\left(r^{-4}\right) \propto r^{-2} \tag{6}$$

Therefore, the relationship between jet cross-sectional radius r and axial position z is $r \propto z^{-\frac{1}{2}}$ in NFES. Due to $r \propto v^{-\frac{1}{2}}$, the relationship between v and z is

$$v \propto z \tag{7}$$

Clearly, from Eq. (7) it can be found that the jet velocity v has a linear relationship with axial position$z$. If $t = 0$ is set at the moment when the jet ejects from the surface of the droplet and $t = T$ is set at the moment when the jet contacts the silicon collector. Then when t ranges in time from 0 to T, the jet acceleration a, the jet velocity v as well as axial position z can be denoted as functions of time, respectively.

$$a = a(t), v = v(t), z = z(t) \tag{8}$$

As the relationship between jet velocity v and axial position z is linear, the following assumption can be made.

$$z = \mathcal{K}v + \mathcal{L} \tag{9}$$

Where $\mathcal{K}$ and $\mathcal{L}$ are the coefficients determined by boundary conditions. And then a differential equation can be acquired according to derivation of both sides of Eq. (9) twice in a row.

$$a = \frac{dv}{dt} = \frac{d^2z}{dt^2} = \mathcal{K}\frac{d^2v}{dt^2} = \mathcal{K}\frac{da}{dt} \tag{10}$$

Obviously, Eq. (10) is a first order ordinary differential equation. So the functions of jet acceleration a, jet velocity v and axial position z depending on time t can be calculated according to Eq. (9) and Eq. (10), respectively.

$$a(t) = exp\left(\frac{t}{\mathcal{K}} + \mathcal{C}\right) \tag{11}$$

$$v(t) = \mathcal{K}\,exp\left(\frac{t}{\mathcal{K}} + \mathcal{C}\right) \tag{12}$$

$$z(t) = \mathcal{K}^2\,exp\left(\frac{t}{\mathcal{K}} + \mathcal{C}\right) + \mathcal{L} \tag{13}$$

Where $\mathcal{C}$, $\mathcal{K}$ and $\mathcal{L}$ are determined by processing parameters. Assuming that at the moment $t = 0, a(0) = exp(\mathcal{C}) = a_0, v(0) = \mathcal{K}, a_0 = v_0, z(0) = \mathcal{K}^2 a_0 + \mathcal{L} = 0$, obviously, $\mathcal{C}, \mathcal{K}$ and $\mathcal{L}$ can be determined by the initial jet acceleration a_0 and the jet velocity v_0. Because $Q = \pi r_0^2 \cdot v_0$, where r_0 is the internal radius of the metallic pipette, the following formulas can be obtained$\mathcal{K} = Q/(\pi r_0^2 \cdot a_0)$,$\mathcal{L} = -Q^2/\left(\pi^2 r_0^4 \cdot a_0\right)$ and $\mathcal{C} = \ln a_0$. Substituting $\mathcal{C}, \mathcal{K}$ and $\mathcal{L}$ with their expressions, the Eqs. (11)–(13) can be reformulated in the following forms.

$$a = exp\left(\frac{\pi r_0^2 \cdot a_0 \cdot t}{Q} + ln\, a_0\right) \tag{14}$$

$$v = \frac{Q}{\pi r_0^2 \cdot a_0} exp\left(\frac{\pi r_0^2 \cdot a_0 \cdot t}{Q} + ln\, a_0\right) \tag{15}$$

$$z = \left(\frac{Q}{\pi r_0^2 \cdot a_0}\right)^2 exp\left(\frac{\pi r_0^2 \cdot a_0 \cdot t}{Q} + ln\, a_0\right) - \frac{Q^2}{\pi^2 r_0^4 \cdot a_0} \tag{16}$$

The Eq. (17) can be derived by combination of Eq. (1) and Eq. (15).

$$r = \left\{ r_0^2 \cdot a_0 \cdot \left\{ exp\left(\frac{\pi r_0^2 \cdot a_0 \cdot t}{Q} + ln\, a_0\right)\right\}^{-1}\right\}^{\frac{1}{2}} \tag{17}$$

By combination of Eqs. (15)–(17), the final expressions for jet velocity v and cross-sectional radius r in terms of the axial position z, volume flow rate Q, initial acceleration of the jet a_0 and the internal diameter of the metallic pipette r_0 are derived.

$$v = \frac{\pi r_0^2 \cdot a_0 \cdot z}{Q} + \frac{Q}{\pi r_0^2} = \frac{a_0}{v_0} z + v_0 \tag{18}$$

$$r = r_0 \left(\frac{\pi^2 r_0^4 a_0}{Q^2} z + 1\right)^{-\frac{1}{2}} = r_0 \left(\frac{a_0}{v_0^2} z + 1\right)^{-\frac{1}{2}} \tag{19}$$

In next section, based on the Slender-body theory and Giesekus model, the relationship between the initial jet acceleration a_0 at the origin of the nozzle and the process parameters of NFES is derived.

III. DERIVATION OF A QUADRATIC EQUATION FOR INITIAL JET ACCELERATION

In section II, the expressions for the jet cross-sectional radius and jet velocity in terms of axial position and initial jet acceleration are derived. In this section, based on Slender-body theory[20,21] and Giesekus model,[22,23] a quadratic equation for initial jet acceleration is acquired using new boundary conditions, of which coefficients are expressed in process parameters of NFES. Here, six dimensionless control equations representing the mass conservation, charge conservation, linear momentum balance, Coulomb's law for the electric field and the tensile force are presented, respectively:[24]

$$\tilde{r}^2 \tilde{v} = 1 \tag{20}$$

$$\tilde{r}^2 \tilde{E} + Pe \tilde{r} \tilde{v} \tilde{\sigma} = 1 \tag{21}$$

$$\tilde{v}\tilde{v}' = \frac{1}{Fr} + \frac{3\left(1 - r_\eta\right)}{Re} \frac{1}{\tilde{r}^2} \frac{d}{d\tilde{z}} \left(\tilde{r}^2 \tilde{v}'\right) + \frac{1}{Re} \frac{T_p'}{\tilde{r}^2} + \frac{1}{We} \frac{\tilde{r}'}{\tilde{r}^2} + \varepsilon \left(\tilde{\sigma}\tilde{\sigma}' + \beta \tilde{E}\tilde{E}' + \frac{2\tilde{\sigma}\tilde{E}}{\tilde{r}}\right) \tag{22}$$

$$\tilde{E}(\tilde{z}) = \tilde{E}_\infty - \ln \chi \left(\frac{d\left(\tilde{\sigma}\tilde{r}\right)}{d\tilde{z}} - \frac{\beta}{2} \frac{d^2\left(\tilde{E}\tilde{r}^2\right)}{d\tilde{z}^2}\right) \tag{23}$$

$$\widetilde{\tau_{prr}} + De\left(\tilde{v}\widetilde{\tau_{prr}}' + \tilde{v}'\widetilde{\tau_{prr}}\right) + \alpha \frac{De}{r_\eta} \widetilde{\tau_{prr}}^2 = -r_\eta \tilde{v}' \tag{24}$$

$$\widetilde{\tau_{pzz}} + De\left(\tilde{v}\widetilde{\tau_{pzz}}' - 2\tilde{v}'\widetilde{\tau_{pzz}}\right) + \alpha\frac{De}{r_\eta}\widetilde{\tau_{pzz}}^2 = 2r_\eta\tilde{v}' \tag{25}$$

The dimensionless quantities are defined as: cross-sectional radius $\tilde{r} = r/r_0$, axial coordinate $\tilde{z} = z/r_0$, jet velocity $\tilde{v} = v/v_0$, electric field $\tilde{E} = E/E_0$, surface charge density $\tilde{\sigma} = \sigma/\sigma_0$, $\widetilde{\tau_{prr}} = \tau_{prr}/\tau_0$, $\widetilde{\tau_{pzz}} = \tau_{pzz}/\tau_0$. Where r_0 is the initial jet radius,$v_0 = Q/(\pi r_0^2)$, $E_0 = I/(\pi r_0^2 K)$, $\sigma_0 = \bar{\epsilon}E_0$ and $\tau_0 = (\eta_0 v_0)/r_0$. The definitions of the dimensionless parameters of Eq. (20)–(25) are as follows: electric peclet number $Pe = 2\bar{\epsilon}v_0/Kr_0$, Froude number $Fr = v_0^2/gr_0$, Reynolds number $Re = \rho v_0 r_0/\eta_0$, Weber number $We = \rho v_0^2 r_0/\gamma$, aspect ratio $\chi = L/r_0$, Deborth number $De = \lambda v_0/r_0$, viscosity ratio $r_\eta = \eta_p/\eta_0$, and $\varepsilon = \bar{\epsilon}E_0^2/\rho v_0^2$, $\beta = \epsilon/\bar{\epsilon} - 1$. L is the distance between the pipette nozzle and collector substrate. At the origin of the jet ($\tilde{z} = 0$), the following boundary conditions are used.

$$\tilde{r}(0) = \lambda, \tilde{v}(0) = \frac{1}{\lambda^2}, \tilde{E}(0) = 1, \tilde{\sigma}(0) = 0, \widetilde{\tau_{prr}} = -r_\eta \cdot \tilde{v}' = 2 \cdot r_\eta \cdot \frac{\tilde{r}'}{\tilde{r}^3}, \widetilde{\tau_{pzz}} = -2 \cdot \widetilde{\tau_{prr}} \tag{26}$$

Here, some explanations should be provided. In other people's models, they all assumed that $\tilde{r}(0) = 1$, but actually the electrified jet does not meet the requirement of Slender-body theory ($|dR(z)/dz| \ll 1$) at the outlet of the pipette. So if $\tilde{r}(0) = 1, \tilde{v}(0) = 1$ are used as boundary conditions, the initial jet acceleration calculated by the proposed model will be much smaller than the actual one. Therefore, in order to use Giesekus model and Slender-body theory to calculate the initial jet acceleration a_0 at the origin of the nozzle, in the model proposed in this paper, $\tilde{r}(0)$ is assumed to be λ. It can be understood that the actual initial jet acceleration a_0 in NFES is equal to that at $\tilde{r} = \lambda$ in the proposed model. Because of $\varepsilon(\tilde{\sigma}\tilde{\sigma}' + \beta\tilde{E}\tilde{E}' + 2\tilde{\sigma}\tilde{E})|_{\tilde{z}=0} \ll \frac{1}{Fr}$, it can be assumed $\varepsilon(\tilde{\sigma}\tilde{\sigma}' + \beta\tilde{E}\tilde{E}' + 2\tilde{\sigma}\tilde{E})|_{\tilde{z}=0} = 0$ to simplify the calculation. Then the Eq. (27) is acquired.

$$\frac{1}{\lambda^2}\tilde{v}' = \frac{1}{Fr} + \frac{3(1-r_\eta)}{Re}\frac{1}{\lambda^2}\frac{d}{d\tilde{z}}(\tilde{r}^2\tilde{v}') + \frac{1}{Re}\frac{1}{\lambda^2}\frac{dT_P}{d\tilde{z}} + \frac{1}{We}\frac{1}{\lambda^2}\frac{d\tilde{r}}{d\tilde{z}} \tag{27}$$

In order to simplify the Eq. (27), $\frac{d}{d\tilde{z}}(\tilde{r}^2\tilde{v}')$, $\frac{dT_P}{d\tilde{z}}$ and $\frac{d\tilde{r}}{d\tilde{z}}$ at $\tilde{z} = 0$ need to be calculated. Because $\tilde{r}^2\tilde{v} = 1$ and $T_P = \tilde{r}^2(\widetilde{\tau_{pzz}} - \widetilde{\tau_{prr}}) = -6r_\eta\frac{\tilde{r}'}{\tilde{r}}$, the Eqs. (28)–(31) can be obtained.

$$\frac{d}{d\tilde{z}}(\tilde{r}^2\tilde{v}') = \frac{d}{d\tilde{z}}\left(\frac{\tilde{v}'}{\tilde{v}}\right) = \frac{\tilde{v}''\tilde{v} - (\tilde{v}')^2}{\tilde{v}^2} \tag{28}$$

$$\frac{dT_P}{d\tilde{z}} = -6r_\eta\frac{\tilde{r}''\tilde{r} - (\tilde{r}')^2}{\tilde{r}^2} \tag{29}$$

$$\frac{d\tilde{r}}{d\tilde{z}} = \frac{d(\tilde{v}^{-\frac{1}{2}})}{d\tilde{z}} = -\frac{1}{2}\tilde{r}^3\tilde{v}' \tag{30}$$

$$\tilde{v}'' = \frac{d^2(\tilde{r}^{-2})}{d\tilde{z}^2} = \frac{6(\tilde{r}')^2}{\tilde{r}^4} - \frac{2\tilde{r}''}{\tilde{r}^3} \tag{31}$$

When $\tilde{z} = 0$, $\tilde{r}''(0)$ is much smaller than $\tilde{r}'(0)$ and can be neglected. The Eqs. (28), (29) and (31) can be reformulated in the following forms.

$$\frac{d}{d\tilde{z}}(\tilde{r}^2\tilde{v}')|_{\tilde{z}=0} = \frac{\lambda^4\left\{\tilde{v}'(0)\right\}^2}{2} \tag{32}$$

$$\left.\frac{dT_P}{d\tilde{z}}\right|_{\tilde{z}=0} = 6r_\eta\left.\frac{(\tilde{r}')^2}{\tilde{r}^2}\right|_{\tilde{z}=0} = \frac{3r_\eta\lambda^4\left\{\tilde{v}'(0)\right\}^2}{2} \tag{33}$$

$$\tilde{v}''(0) = \frac{6(\tilde{r}')^2}{\tilde{r}^4}|_{\tilde{z}=0} = \frac{3\lambda^2\left\{\tilde{v}'(0)\right\}^2}{2} \tag{34}$$

From the Eqs. (27)–(34), the Eq. (35) can be derived.

$$\frac{3\lambda^2}{2Re}\left\{\tilde{v}'(0)\right\}^2 - \left(\frac{1}{\lambda^2} + \frac{\lambda}{2We}\right)\tilde{v}'(0) + \frac{1}{Fr} = 0 \tag{35}$$

The Eq. (35) is a quadratic equation for initial jet acceleration with its coefficients expressed in terms of the process parameters and boundary conditions in NFES. Obviously, the $\tilde{v}'(0)$ here is dimensionless and a_0 in Eq. (19) is dimensional. In order to acquire the final dimensionless result, the following equations are given.

$$\tilde{v}' = \frac{d\tilde{v}}{d\tilde{z}} = \frac{r_0}{v_0} \cdot \frac{dv}{dz} \tag{36}$$

$$a = \frac{dv}{dt} = \frac{dv}{dz} \cdot \frac{dz}{dt} = v \cdot \frac{dv}{dz} = \frac{v \cdot v_0}{r_0} \cdot \tilde{v}' \tag{37}$$

The initial jet acceleration a_0 can be expressed in the following form:

$$a_0 = \frac{v_0^2}{r_0} \cdot \tilde{v}'(0) \tag{38}$$

In section II, the cross-sectional radius of the jet r is expressed as$r = r_0\left(\frac{\pi^2 r_0^4 a_0}{Q^2}z + 1\right)^{-\frac{1}{2}}$. By changing it into dimensionless form based on $\tilde{r} = \frac{r}{r_0}$ and $\tilde{z} = \frac{z}{r_0}$, it is

$$\tilde{r} = \left\{\tilde{v}'(0) \cdot \tilde{z} + 1\right\}^{-\frac{1}{2}}. \tag{39}$$

Inserting the Eq. (39) into the Eq. (20), it is

$$\tilde{v} = \tilde{v}'(0) \cdot \tilde{z} + 1 \tag{40}$$

So far, the dimensionless exponential functions of jet cross-sectional radius $\tilde{r}$ and jet velocity $\tilde{v}$ are derived in terms of axial position $\tilde{z}$. And a quadratic equation is provided to calculate the dimensionless initial jet acceleration $\tilde{v}'(0)$ with its coefficients expressed in terms of the processing parameters in NFES.

IV. EXPERIMENTS AND DISCUSSIONS

A. Materials and process parameters

Polyethylene oxide (PEO, molecular weight $M = 10^6$g/mol) is used as the experimental materials to prepare the solutions, of which concentration is 4wt%. The PEO is dissolved in a mixture of around 60% deionized water and 40% ethanol and stirred at room temperature (about 20 °C) for 24 hours.

All of the parameters listed in Table I are provided by Hohman *et al.*[25] and Fong *et al.*.[26]

B. Experimental setup

The schematic illustration of the apparatus for NFES is shown in Figure 1. A metallic pipette with an internal diameter of about 160 μm is used to produce polymer fibers. A precise syringe pump (KD Scientific Inc, Holliston, America) supplies a steady flow of solution to the pipette. A power supply (Dongwen High-Voltage Power Supply, Tianjin, China) provides the high voltage up to 60 kv. An X-Y motorized stage (ProScan TM, Prior Scientific Inc., UK) is applied to collect precisely deposited polymer fibers. A microscope (Nikon ECLIPSE Ti-E, Nikon, Tokyo, Japan) and a CCD (RENUSCO DTM-300, Suzhou, China) are used to observe the electrified jet in space. The distance

TABLE I. Process parameters of 4wt% PEO solutions used in experiments.

Symbol	Definition	
$\boldsymbol{\rho}$	density	$1.2 \times 10^3 kg \cdot m^{-3}$
$\boldsymbol{\epsilon}/\bar{\epsilon}$	dielectric constant	42.7
$\boldsymbol{\eta_0}$	viscosity	$12.5P$
$\boldsymbol{\gamma}$	surface tension coefficient	$76.6 dyn \cdot cm^{-1}$
$\boldsymbol{K}$	electric conductivity	$4.902 \times 10^{-3} S \cdot m^{-1}$
$\boldsymbol{\eta_s}$	solvent viscosity	$10^{-2} P$
$\bar{\boldsymbol{\epsilon}}$	dielectric constant of the ambient air	$8.854 \times 10^{-12} C^2/N \cdot m^2$

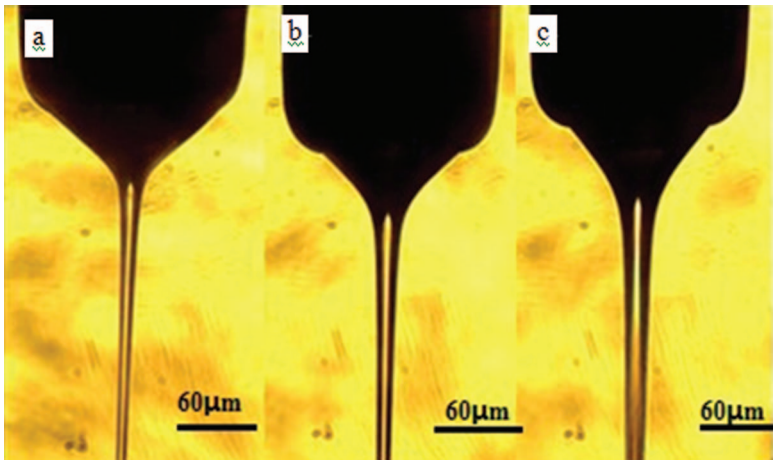

FIG. 2. Video graphs of electrified jets under different flow rate: (a) $r_0 = 80um$, $Q = 0.3ml/h$ (b) $r_0 = 80um$, $Q = 0.6ml/h$ (c) $r_0 = 80um$, $Q = 0.9ml/h$.

between the pipette nozzle and collector substrate L is 3 mm and the applied voltage is about 1500 V.

C. Comparison between theoretical analysis and experimental results

To verify the correctness of the proposed model, three groups of experiments are conducted through the use of 4wt% PEO solutions. In each set of experiments, the same metallic pipettes with the internal diameters (160μm) are used, but the volume flow rates Q are different (0.3 ml/h, 0.6 ml/h and 0.9 ml/h, respectively). The images of electrospinning jets of experiments are shown in Figure 2. We obtained the velocity r of charged jet indirectly. Firstly, the cross-sectional radius r is obtained by using Markman software to measure the diameter of polymer fiber based on image measurement method. Then$v$ can be acquired according to $\tilde{r}^2\tilde{v} = 1$, $\tilde{r} = r/r_0$, $\tilde{v} = v/v_0$. Figures 3–5 show the comparison between theoretical curves and experimental results.

It can be seen from Figures 3–5 that the theoretical curves is not in accordance with experimental results when $z/r_0 \leq 1$. However, the initial stage ($z/r_0 \leq 1$) are not important to predict the radius of the electrified jet. The final value of z/r_0 is much larger than 1 in the stretching stage. When $z/r_0 > 1$, the theoretical curves and experimental results are coincident. The velocity v and cross-sectional radius r of charged jet can be obtained. Theoretical predictions and experimental results about v and r at $z/r_0 = 3.5$ are listed in Table II.

When the polymer fibers approach the collector, we focus on the final velocity and radius charged jet that decided the radius of polymer fibers and the motion of collector. In NFES, the final diameters of the jet are determined by the stretching stage rather than the initial stage. When $z/r_0 > 1$, the proposed model can be used to predict the final velocities of the polymer fiber accurately. To collect straight-line-shape polymer fibers, the collector stage should move at an

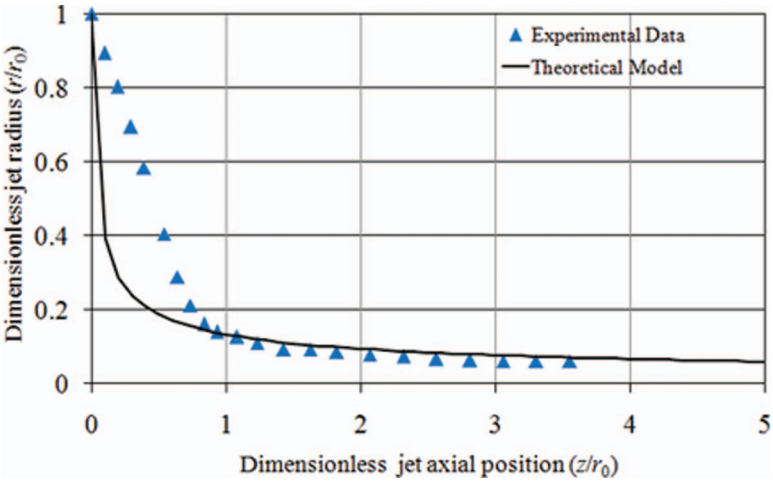

FIG. 3. Comparison between theoretical curve and experimental data under the condition that $Q = 0.3$ *ml/h*. The parameters used by our prediction are as follows: $\chi = 37.5$, $\beta = 41.7$, Fr $= 0.022$, We $= 0.215 \times 10^{-4}$, Re $= 0.32 \times 10^{-4}$, $\lambda = 0.1$, $\tilde{v}'(0) = 55.24$.

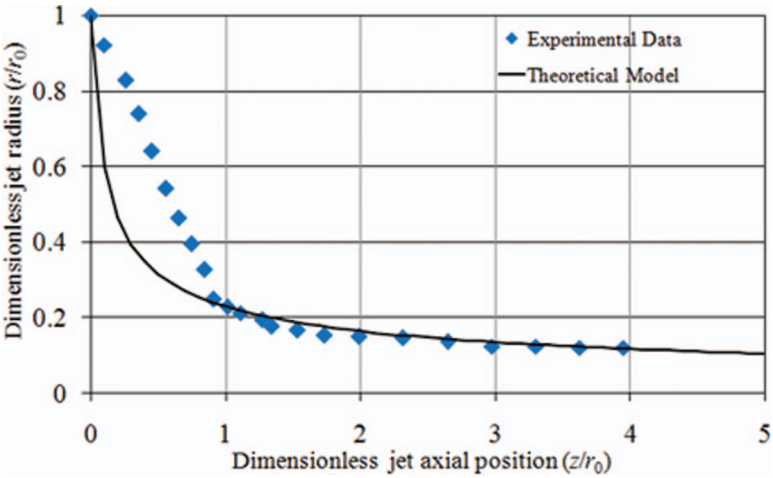

FIG. 4. Comparison between theoretical curve and experimental data under the condition that $Q = 0.6$ ml/h. The parameters used by our prediction are as follows: $\chi = 37.5$, $\beta = 41.7$, Fr $= 0.088$, We $= 0.86 \times 10^{-4}$, Re $= 0.64 \times 10^{-4}$, $\lambda = 0.125$, $\tilde{v}'(0) = 18.11$.

TABLE II. Theoretical predictions and experimental results at $z/r_0 = 3.5$.

	r (μm)		v (*m/s*)	
Q (*ml/h*)	Theoretical analysis	Experimental results	Theoretical analysis	Experimental results
0.3	4.96	5.74	1.08	0.81
0.6	9.76	10.00	0.56	0.53
0.9	13.04	14.72	0.47	0.37

appropriate velocity determined by the final velocity of polymer fibers. When the electrospinning velocity of polymer fiber is faster than the collector moving velocity, the polymer fiber will spiral locally. When the collector stage moves faster than the electrospinning velocity, the polymer fiber will diminish gradually. The proposed mathematical model based on exponential functions can be used to predict the behavior of the electrified jet in NFES. According to the model, the final

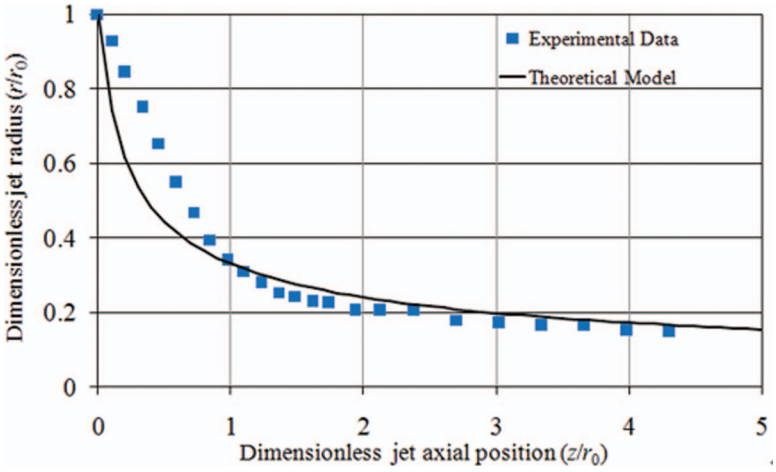

FIG. 5. Comparison between theoretical curve and experimental data under the condition that $Q = 0.9$ *ml/h*. The parameters used by our prediction are as follows: $\chi = 37.5$, $\beta = 41.7$, Fr $= 0.198$, We $= 1.935 \times 10^{-4}$, Re $= 0.96 \times 10^{-4}$, $\lambda = 0.15$, $\tilde{v}'(0) = 8.18$.

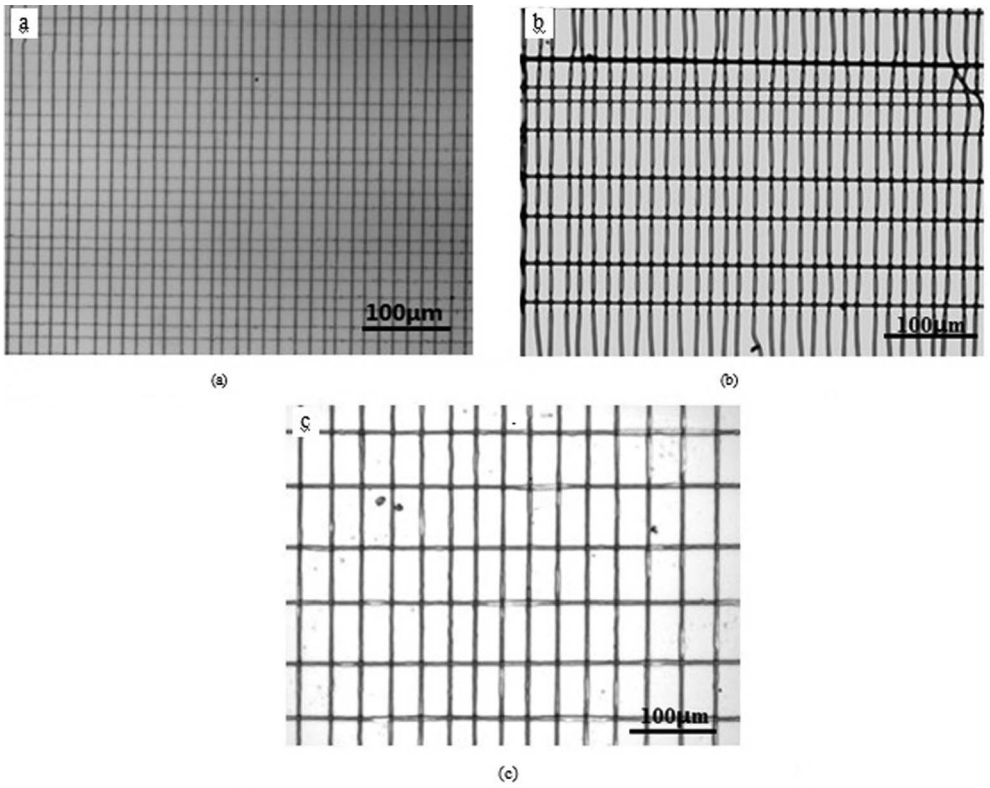

FIG. 6. Precise deposition of polymer fibers. (a) The radius of the polymer fiber is about 1.8 μm at the velocities 8.59 *m/s*. (b) The radius of the polymer fiber is about 3.0 μm at the velocities 5.63 *m/s* (c). The radius of the polymer fiber is about 4.5 μm at the velocities 3.82 *m/s*.

cross-sectional radius of the polymer fiber and velocity of the jet could be calculated. By applying the equation of $\tilde{r}_{final} = \{\tilde{v}'(0) \cdot \chi + 1\}^{-\frac{1}{2}}$ and $\tilde{v}_{final} = \tilde{v}'(0) \cdot \chi + 1$, the final radius r_{final} of the polymer fiber are 1.75 μm, 3.07 μm and 4.56 μm in Figure 6, respectively. Correspondingly, the final velocities v_{final} are 8.89 m/s, 5.63 m/s and 3.82 m/s, respectively.

V. CONCLUSION

In this paper, to analyze the behavior of charged jet in NFES using a mathematical model, the momentum balance equation was simplified, and a new expression between jet cross-sectional radius and axial position was derived. Using this new expression and mass conservation equation, expressions for jet cross-sectional radius and jet velocity were derived in terms of axial position and initial jet acceleration in the form of exponential functions. To calculate the initial jet acceleration, the control equations based on Slender-body theory and Giesekus model were introduced, and a quadratic equation for initial jet acceleration was acquired with its coefficients expressed in terms of the process parameters in NFES. After experimental verification, the theoretical curves and experimental results were found to be in perfect agreement in $z/r_0 > 1$. This proposed mathematical model has several advantages and has important guiding significance to precise deposition of polymer fibers. Firstly, it will be able to accurately predict the diameter and velocity of polymer fibers in NFES. Secondly, it will be able to apply mathematical analysis rather than experimental methods to study the effects of the process parameters in NFES. Thirdly, it will be able to regulate the movement velocity of collector stage according to mathematical model rather than experience. So the precise deposition of polymer fibers in NFES will be more accurate and convenient, and with the theoretical model proposed in this paper, real-time controllable NFES is possible to be realized.

ACKNOWLEDGMENT

This work was financially supported by National Natural Science of China (Grant No. 61233010), Instrument Development Major Program of National Natural Science of China (Grant No. 61327811), Jiangsu Natural Science Founds for Distinguished Young Scholar (Grant No. BK2012005), and Qing Lan Project of Jiangsu Province.

[1] Y. C. Ahn, S. K. Park, G. T. Kim, Y. J. Hwang, C. G. Lee, H. S. Shin, and J. K. Lee, "Development of high efficiency nanofilters made of nanofibers," Current Applied Physics. **6**(6), 1030 (2006).
[2] S. Y. Chew, R. Mi, A. Hoke, and K. W. Leong, "The effect of the alignment of electrospun fibrous scaffolds on Schwann cell maturation," Biomaterials. **29**(6), 653 (2008).
[3] M. Grätzel, "Dye-sensitized solid-state heterojunction solar cells," MRS Bull. **30**(1), 23 (2005).
[4] H. J. Jin, S. V. Fridrikh, G. C. Rutledge, and D. L. Kaplan, "Electrospinning Bombyx mori silk with poly (ethylene oxide)" Biomacromolecules. **3**(6), 1233 (2002).
[5] W. Cui, Y. Zhou, and J. Chang, "Electrospun nanofibrous materials for tissue engineering and drug delivery," Science and Technology of Advanced Materials. **11**(1), 014 (2010).
[6] J. S. Im, S. C. Kang, S. H. Lee, and Y. S. Lee, "Improved gas sensing of electrospun carbon fibers based on pore structure, conductivity and surface modification" Carbon. **48**(9), 2573 (2010).
[7] C. Chang, V. H. Tran, J. Wang, Y. K. Fuh, and L. Lin, "Direct-write piezoelectric polymeric nanogenerator with high energy conversion efficiency," Nano letters. **10**(2), 726 (2010).
[8] G. Taylor, "Electrically driven jets," Proceedings of the Royal Society of London. A. Mathematical and Physical Sciences. **313**(1515), 453 (1969).
[9] J. J. Feng, "The stretching of an electrified non-Newtonian jet: A model for electrospinning," Physics of Fluids. **14**(39), 12 (2002).
[10] B. Sundaray, V. Subramanian, T. S. Natarajan, R. Z. Xiang, C. C. Chang, and W. S. Fann, "Electrospinning of continuous aligned polymer fibers," Applied physics letters. **84**(7), 1222 (2004).
[11] W. E. Teo, M. Kotaki, X. M. Mo, and S. Ramakrishna, "Porous tubular structures with controlled fibre orientation using a modified electrospinning method," Nanotechnology. **16**(6), 918 (2005).
[12] N. Bhattarai, D. Edmondson, O. Veiseh, F. A. Matsen, and M. Zhang, "Electrospun chitosan-based nanofibers and their cellular compatibility," Biomaterials. **26**(31), 6176 (2005).
[13] W. E. Teo and S. Ramakrishna, "Electrospun fibre bundle made of aligned nanofibres over two fixed points," Nanotechnology. **16**(9), 1878 (2005).
[14] P. Katta, M. Alessandro, R. D. Ramsier, and G. G. Chase, "Continuous electrospinning of aligned polymer nanofibers onto a wire drum collector," Nano Letters. **4**(11), 2215 (2004).
[15] J. A. Matthews, G. E. Wnek, D. G. Simpson, and G. L. Bowlin, "Electrospinning of collagen nanofibers," Biomacromolecules. **3**(2), 232 (2002).
[16] D. Sun, C. Chang, S. Li, and L. Lin, "Near-field electrospinning" Nano letters. **6**(4), 839 (2006).
[17] C. Chang, K. Limkrailassiri, and L. Lin, "Continuous near-field electrospinning for large area deposition of orderly nanofiber patterns," Applied Physics Letters. **93**(12), 123111 (2008).
[18] G. S. Bisht, G. Canton, A. Mirsepassi, L. Kulinsky, S. Oh, D. Dunn-Rankin, and M. J. Madou, "Controlled continuous patterning of polymeric nanofibers on three-dimensional substrates using low-voltage near-field electrospinning," Nano letters. **11**(4), 1831 (2011).

[19] J. H. He, Y. Liu, L. F. Mo, Y. Q. Wan, and L. Xu, *Electrospun Nanofibres and Their Applications* (ISmithers, Shawbury, UK, 2008)
[20] M. M. Denn, C. J. Petrie, and P. Avenas, "Mechanics of steady spinning of a viscoelastic liquid," AIChE Journal **21**(4), 791 (1975).
[21] A. Calvo and A. Gan, "On the theory of electrohydrodynamically driven capillary jets," Fluid Mech. **335**, 165 (1997).
[22] R. B. Bird, R. C. Armstrong, and O. Hassager, "Dynamics of Polymeric Liquids," Physics Today. **1**, 31 (1978).
[23] H. Giesekus, "A simple constitutive equation for polymer fluids based on the concept of deformation dependent tensorial mobility," Journal of Non-Newtonian Fluid Mechanics. **11**(1), 69 (1982).
[24] J. J. Feng, "Stretching of a straight electrically charged viscoelastic jet," Journal of Non-Newtonian Fluid Mechanics. **116**(1), 55 (2003).
[25] M. M. Hohman, M. Shin, G. Rutledge, and M. P. Brenner "Electrospinning and electrically forced jets. I. Stability theory," Physics of Fluids. **13**, 2201 (2001).
[26] H. Fong, I. Chun, and D. H. Reneker, "Beaded nanofibers formed during electrospinning," Polymer. **40**(16), 4585 (1999).